ACS APPLIED MATERIALS & INTERFACES

Research Article

www.acsami.org

Ultralightweight Silver Nanowires Hybrid Polyimide Composite Foams for High-Performance Electromagnetic Interference Shielding

Jingjing Ma, Maosheng Zhan,* and Kai Wang

Key Laboratory of Aerospace Materials and Service of Ministry of Education, School of Materials Science and Engineering, Beihang University, Beijing 100191, People's Republic of China

ABSTRACT: Ultralightweight silver nanowires (AgNWs) hybrid polyimide (PI) composite foams with microcellular structure and low density of 0.014−0.022 g/cm^3 have been fabricated by a facile and effective one-pot liquid foaming process. The tension flow generated during the cell growth induced the uniform dispersion of AgNWs throughout the cell walls. The interconnected AgNWs network in the cell walls combined with the large 3D AgNWs network caused by 3D structure of foams provided fast electron transport channels inside foams. The electromagnetic interference (EMI) shielding effectiveness (SE) of these foams increased with increasing AgNWs loading as well as the nanowire aspect ratio due to the increasing connections of the conduction AgNWs network. Appropriate surface treatment like etching or spraying facilitated the construction of the seamlessly interconnected 2D AgNWs network on the surface, which could effectively reflect electromagnetic waves. Maximum specific EMI SE of values of 1210 dB·g^{-1}·cm^3 at 200 MHz, 957 dB·g^{-1}·cm^3 at 600 MHz, and 772 dB·g^{-1}·cm^3 at 800−1500 MHz were achieved in sprayed composite foams containing <0.044 vol % AgNWs loading, which far surpasses the best values of other composite materials. The reflections of interconnected AgNWs networks on the surface and inside foams combined with the multiple reflections at interfaces contributed to the shielding effect.

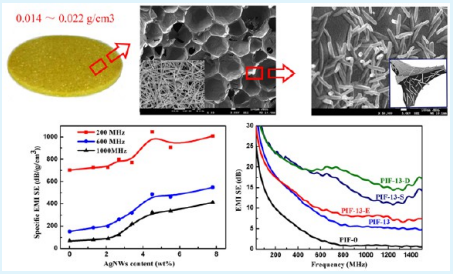

KEYWORDS: *silver nanowires, polyimide foam, microcellular structure, interconnected network, electromagnetic interference shielding*

1. INTRODUCTION

Recently, considerable attention has been devoted to the development of high-performance electromagnetic interference (EMI) shielding materials due to the electromagnetic pollution generated by the rapid development of telecommunications and electronics.[1−3] Being lightweight is an important technical requirement for practical EMI shielding applications, especially in areas of aerospace, automobiles, and household appliances.[4,5] Foamed composites with cell structures are excellent candidates for preparing lightweight EMI shielding materials.[6,7] For example, Cu−Ni alloy foam integrated with carbon nanotubes (CNTs)[8] or graphene,[9] and carbon foam with metal surface[10] or ferrocene[11] are effective lightweight foamed EMI shielding materials. Compared to the foamed composites mentioned above, polymer composite foams[12−14] have advantages such as low density, good processability, tunable conductivity, and resistance to corrosion. The main approach to produce polymeric foams for EMI shielding is to add some conductive nanoparticles such as CNTs, graphene, carbon fiber, carbon black,[15] and conductive polymer[16] into the polymer foam matrix. For example, Yang et al.[17,18] used a chemical blowing agent to fabricate polystyrene (PS)/15 wt % carbon nanofiber composite foams and achieved a EMI shielding effectiveness (SE) of 19 dB at 8.2−12.4 GHz. Meanwhile, they developed PS/CNTs foam that exhibited a specific EMI SE (EMI SE divided by the density) of 33.1 dB·g^{-1}·cm^3 for 7 wt % nanotube loading in the frequency range of 8.2−12.4 GHz. Afterward, Yan et al.[19] reported PS/graphene foams with a specific EMI SE of 64.4 dB·g^{-1}·cm^3 for 30 wt % graphene loading at 8.2−12.4 GHz. Meanwhile, Zhang et al.[20] used supercritical CO_2 as a physical blowing agent to fabricate poly(methyl methacrylate) (PMMA)/graphene foams that exhibited a specific EMI SE of 17−25 dB·g^{-1}·cm^3 in 5 wt % graphene at 8.2−12.4 GHz. Afterward, Ling et al.[21] reported poly(ether imide) (PEI)/graphene foams with a specific EMI SE of 44 dB·g^{-1}·cm^3 at 10 wt % graphene loading using a phase separation process. Recently, Shen et al.[22] also used the phase separation process to fabricate PEI/graphene@Fe_3O_4 with 42 dB·g^{-1}·cm^3 in 10 wt % graphene@Fe_3O_4 loading at 8−12 GHz. Recently, Ameli et al.[23,24] fabricated polypropylene (PP)/nanofillers foams using foaming injection molding. They found that the specific EMI SE values were 34 dB·g^{-1}·cm^3 for 10 vol % carbon nanofiber loading and 75 dB·g^{-1}·cm^3 for 1.5 vol % stainless-steel fiber loading at 8−12 GHz, respectively.

However, there are still some disadvantages that restrict the development of these polymer composite foams for high-performance EMI shielding materials. First, in most cases, a relatively high content of nanofillers like 15 wt % nanofiber, 30 wt % graphene, or 10 wt % graphene@Fe_3O_4 is needed to approach the target value of the EMI SE required for commercial applications around 20 dB, which may decrease the mechanical properties because of severe aggregation.

Received: October 1, 2014
Accepted: December 17, 2014
Published: December 17, 2014

DOI: 10.1021/am5067095
ACS Appl. Mater. Interfaces 2015, 7, 563−576

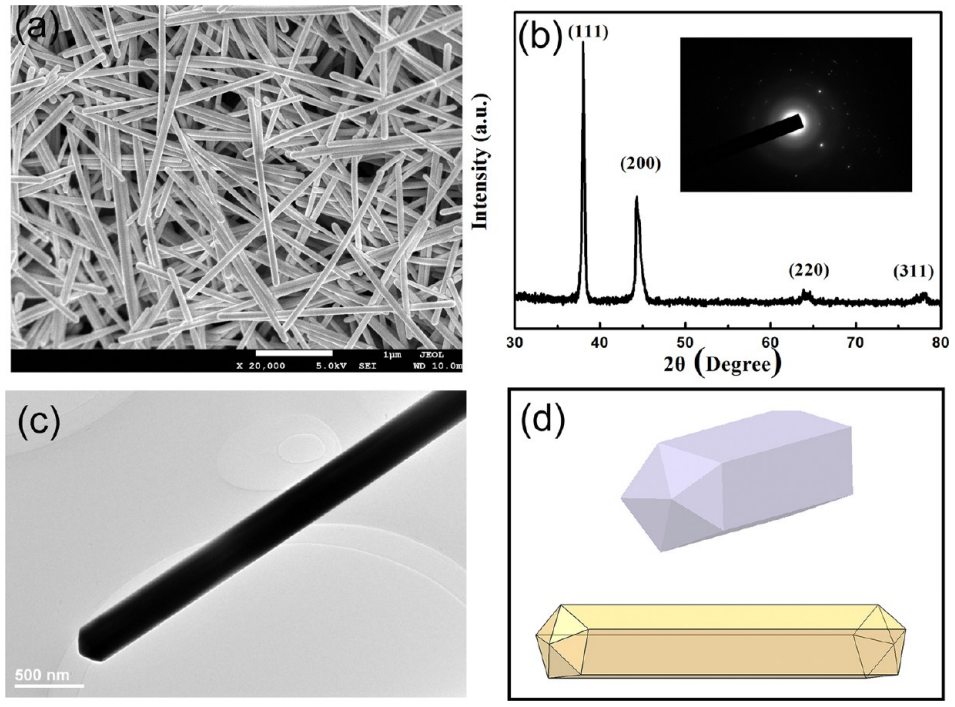

Figure 1. Structural characterization of the as-synthesized AgNWs: (a) FESEM images of nanowires, (b) XRD pattern of the AgNWs, inset shows the selected area electron diffraction (SAED) of a single silver nanowire, (c) TEM image of single silver nanowire, and (d) morphology model of AgNWs.

Second, the conventional polymers such as PP, PMMA, PS, PEI, and polyurethane (PU)[25] exhibit low heat-resistance, poor flame retardancy and short lifetime, which restrict their use as the EMI shielding materials in advanced fields and other special applications for electronics. In addition, their density higher than 0.08 g/cm^3 make the specific EMI SE of most composite foams be only a few times larger than that of metal-based foam materials, which is unfavorable for applications that need lightweight materials. As a consequence, it will be highly desirable to develop ultralightweight polymer foams with a low nanofiller loading exhibiting higher-temperature stability, ultralightweight and ultrahigh specific EMI SE for high-performance EMI shielding applications by a low-cost, efficient, and facile process.

Compared to conventional carbon-based nanofillers, metal nanowires possess high electrical conductivity, and their properties dependent upon structures can be controlled by the synthesis conditions.[26] Importantly, a low content of nanowires is required to form an interconnected network in the polymer matrix and to achieve the target properties of composites due to their high aspect ratio of 20−500.[27] Hence, it is postulated that metal nanowires are promising nanofillers instead of carbon-based nanofillers for EMI shielding. Gelves et al.[28] fabricated PS/Cu nanowires composites exhibiting EMI SE of 20 dB with only 1.3 vol % Cu nanowires content at 8−12 GHz. Among all metal nanowires, silver nanowires[29−31] (AgNWs) exhibit the highest conductivity of 6.3 × 10^7 S/m and excellent connectivity with each other. Hu et al.[32] fabricated PES/AgNWs/PET sandwich-structured film with EMI SE of 25 dB at 8−12 GHz by drawn-down rod-coating technology. Yu et al.[33] prepared AgNWs/epoxy resin composites that showed EMI SE of 20 dB at 3−17 GHz. We believe that an extremely low loading (<0.1 vol %) of AgNWs will give polymer composite foams outstanding EMI shielding performance due to their high aspect ratio, high electrical conductivity, and connectivity. More specially, controllable high-concentration AgNWs have been synthesized rapidly on a large scale by a facile and effective two-step dropping polyol method in our previous study.[34] In addition, polyimide foam (PIF),[35−37] a kind of advanced polymer foam, exhibits high temperature resistance, excellent aging resisting, a high glass transition temperature (Tg) of 292 °C, good flame retardancy, and ultralow density of 0.013−0.024 g/cm^3. Thus, it is very valuable to select PIF as the polymer foam matrix to fabricate high-performance EMI shielding materials. Consequently, the combination of the two concepts, AgNWs and PIF are very promising for the design of EMI shielding materials with ultralightweight, higher-temperature stability, long lifetime, and high specific EMI SE. Moreover, polyimide (PI), which can be used as a kind of adhesive, may stick to AgNWs tightly, so that AgNWs could not peel off easily due to the excellent adhesion between PI matrix and metals.[38]

Furthermore, there are few studies available in the literature on the EMI SE of polymer composite foams in the frequency range of 30 MHz−1.5 GHz, but in these studies introduced above, the EMI SE values were characterized at 8−12 GHz, which were usually studied for military applications such as radar, broadcasting satellites, vehicular detection, defense tracking, and weather satellite.[39−41] In consideration of the radiation frequency for common household appliances like 300−450 MHz for computer, 600−1400 MHz for telephone, 30 MHz for television, 30 MHz for washing machines, and 250−380 MHz for cordless phones, it will be of great significance to study the EMI SE in the low frequency of 30 MHz−1.5 GHz. This will help develop high-performance EMI shielding materials for household appliances to effectively protect against the electromagnetic pollution.

DOI: 10.1021/am5067095
ACS Appl. Mater. Interfaces 2015, 7, 563−576

In this study, our aim is to construct conductive networks on a large-scale in composite foams at an extremely low nanofiller loading for high-performance EMI shielding materials. Herein, a series of AgNWs/polyimide hybrid composite foams were fabricated by one-pot liquid foaming process. A composite foam surface was subjected to chemical etching with a mixture of NaOH and ethanol as the etchant so that AgNWs were exposed. To further enhance the foam's EMI shielding properties, AgNWs were also used to form an enhanced coating on the surface by spraying. The morphology and the EMI SE at 30 MHz−1.5 GHz of composite foams at various AgNWs loadings or AgNWs aspect ratios, composite foams subjected to etching, and composite foams coated with AgNWs were investigated. Moreover, the distribution of AgNWs in cells and the shielding mechanism were also demonstrated. To the best of our knowledge, few studies have declared the fabrication of lightweight AgNWs/polyimide composite foams with the combination of higher-temperature stability, ultralightweight, and effective EMI shielding. This study provided a fast, highly reproducible, and scalable technique for the production of functional polyimide foams as EMI shielding materials used in the advanced civil fields such as electronic communications, and household appliances.

2. EXPERIMENTAL SECTION

2.1. Materials. $AgNO_3$, NaCl, $FeCl_3{\cdot}6H_2O$, acetone, and ethanol were all supplied by Beijing Finechem, China. Ethylene glycol (EG) and polyvinylpyrolidone (PVP, Mw ≈ 40 000) were purchased from Xilong Chemical Industry Incorporated Co. Ltd., China. 3,3′,4,4′-Benzophenonetetracarboxylic dianhydride (BTDA) was acquired from Beijing Multi Technology Co. Ltd., China, and was dried in a vacuum oven at 180 °C for 8−10 h prior to use. Polyaryl polymethylene isocyanate (PAPI, PM-200) was obtained from Yantai Wanhua Polyurethanes Co. Ltd., China. Silicone oil (DC-193) was purchased from Foshan Daoning Chemical Co. Ltd., China, and it was the main surfactant. Polyethylene glycol 600 (PEG-600), *N*,*N*′-Dimethylformamide (DMF), methanol, and deionized water were all supplied by Beijing Finechem, China. All chemicals were analytical grade and used without further purification.

2.2. Preparation of AgNWs. A series of AgNWs with different aspect ratios were synthesized by the two-step dropping polyol process, as previously reported by our group.[34] In the typical synthesis procedure, 40 mL of 0.56 M PVP solution in EG was heated to 160 °C until the temperature was steady. Afterward, 100 μL of 0.15 M NaCl solution in EG was injected in the mixture above. Then 10 mL of 1.5 M $AgNO_3$ solution in EG was added into the dropping funnel and then dropped into the flask at the rate of 15 μL/s at first. Once the reaction solution turned to gray, which indicated the presence of silver nanoparticles and pentagonal twinned decahedron particles, all the remaining $AgNO_3$ solution was added into the flask immediately. After 2 h, the reaction was quenched and the suspension was diluted with ethanol (in a weight ratio of 1:10) and centrifuged three times at 8000 rpm for 20 min. The final products were dispersed in DMF and stored at room temperature for further use. The average diameter and length of the nanowires were found to be 90 nm and 7.1 μm (seen Figure 1a), respectively. Moreover, the as-synthesized AgNWs in this study exhibited face-centered-cubic (FCC) crystal structure (JCPDS File 04-0783) (shown Figure 1b) and pentagonal cross section (shown Figure 1c,d). The lattice constant calculated from this XRD pattern according to the lattice spacing of the (111) planes was 4.102 Å, which was very close to the reported data value of 4.0862 Å. Obviously, the ratio of intensity between (111) and (200) peaks showed a relatively high value of 2.88 (the theoretical ratio is 2.5), suggesting the enrichment of (111) crystalline planes in the AgNWs.

2.3. Preparation of AgNWs/Polyimide Hybrid Composite Foams. AgNWs/polyimide in situ hybrid composite foams were prepared by one-pot liquid foaming process according to our previous technique with some modifications.[37] First, a predetermined amount of AgNWs was dispersed in 100 pphp (parts per hundred parts of anhydride by weight) of DMF using a bath sonicator for 60 min in order to achieve optimum dispersion and extensive surface contact with polymer matrix. The AgNWs solution was then added to a 250 mL volume flask under N_2 at approximately 85 °C. Afterward, 100 pphp of BTDA, 40 pphp of processing aids (methanol, DC-193 and PEG-600), and 13 pphp of deionized water were accurately weighted and added to the mixture above. The mixture was stirred for 2 h to give a homogeneous solution named as first solution containing AgNWs. When the first solution was cooled to 25 °C, 200 pphp of PAPI was added to the first solution. The mixture of first solution and PAPI was stirred with a high speed mixer (about 2000 rpm) for 5−15 s. Then it was immediately transferred to a mold where it was allowed to rise freely for 5 min. Once the foam was no longer tacky, it was placed in a vacuum oven at 250 °C to posture for 2 h in order to complete the imidization reaction. High-temperature treatment also could promote effective connections between AgNWs. In this experiment, the AgNWs loadings were 3 pphp, 5 pphp, 8 pphp, 10 pphp, 13 pphp, 15 pphp, and 20 pphp. They were identified as PIF-3, PIF-5, PIF-8, PIF-10, PIF-13, PIF-15, and PIF-20, respectively, in which AgNWs with average diameter of 90 nm and length of 7.1 μm were used. Pure polyimide foam named PIF-0 was also fabricated as the comparative test. According to the composition of PIF-13, a series of composite foams varying in AgNWs aspect ratio (R) were fabricated. And they were designated as PIF-13 (R = 79), PIF-13-2 (R = 47), PIF-13-3 (R = 34), and PIF-13-4 (R = 25), respectively. The chemical reaction that might occur during the preparation was similar to that of our previous study.[37] PIF-8, PIF-13, and PIF-20 were selected to be chemical etched by a NaOH and ethanol mixture for 5 h, and the samples were named as PIF-8-E, PIF-13-E, and PIF-20-E, respectively. Two PIF-13 samples were selected to spray AgNWs on their surfaces by physical spraying method using a Royalmax airbrush at room temperature in which the AgNWs with diameter of 90 nm and length of 7.1 μm were used. In consideration of the adhesion between the coated AgNWs and PI matrix, collected AgNWs were finally dispersed uniformly in dilute polyamic acid to form AgNWs solution with an optimized concentration of 5 mg/mL. The nozzle diameter was 0.2 mm, and the distance between needle and surface was 5 cm. The foam with one surface sprayed with AgNWs was named as PIF-13-S, and the other one with both surface sprayed with AgNWs was expressed as PIF-13-D in which the surface density of the AgNWs coating was 2 mg/cm^2. Judging from the appearance, there were no foaming slags and AgNWs peeling off from PI matrix among all the composite foams.

2.4. Characterization. The foam density was measured as the sample weight divided by its volume according to ASTM D328. The results were the average with standard deviation of at least five different foam samples for each composite foam. The morphology of samples was carried out with field-emission scanning electron microscopy (FESEM, JSM 7500, JEOL) operated at an accelerating voltage of 5 kV after sputter-coating specimens with platinum. The diameters of cells were determined by individually measuring the sizes of 50 cells from the FESEM images with the aid of SISAC-IAS image analyzer. And the diameters and lengths of the AgNWs were also determined by measuring the sizes of 100 nanostructures from the FESEM images. Results are given as averages with standard deviations. The open cell content of composite foams was measured by a picnometer (3H-2000TD-K, BeiShiDe Instrument S&T Co. Ltd.) according to ASTM D6226. Samples were cut into a cuboid (5 × 2.5 × 2.5 cm) to fit a steel container. The reported results were the averages with standard deviations of three tested samples for each composite foam. The apparent viscosity of first solution was measured using a digital viscometer (NDJ-8S, Shanghai Nirun Intelligent Technology Co. Ltd.) at 25 °C. The chemical composites were analyzed with an energy dispersive analyzer (EDS, Oxford Inca). A schematic diagram of the SE measurement setup (DN 1015) is displayed in Figure 2 in which a network analyzer was employed. EMI SE was measured at room temperature in the frequency range of 30 MHz−1.5 GHz

DOI: 10.1021/am5067095
ACS Appl. Mater. Interfaces 2015, 7, 563−576

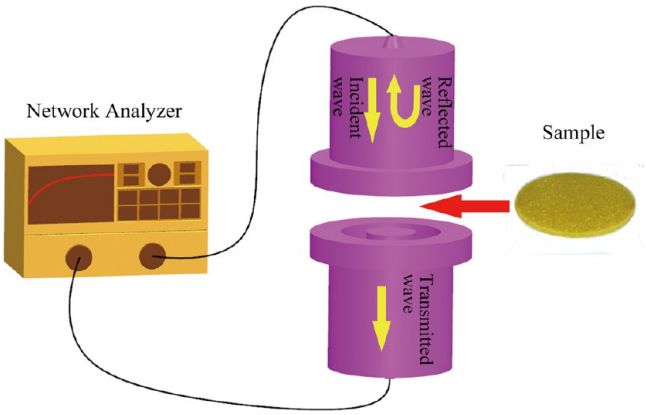

Figure 2. Schematic diagram of the shielding effectiveness measurement setup.

according to ASTM D4935-2010. The samples were cut to disk with diameter of 115 mm and thickness of 5 mm.

3. RESULTS AND DISCUSSTION

3.1. Morphology Characterization of AgNWs/PI Composite Foams.

3.1.1. Cell Morphology Characterization of AgNWs/PI Composite Foams. Table 1 shows the density of AgNWs/polyimide hybrid composite foams and their actual loading of AgNWs in this study. As shown in Table 1, the density of pure PIF was 0.014 g/cm^3. And the density of AgNWs/polyimide composite foams was 0.016−0.022 g/cm^3, suggesting that the introduction of AgNWs did not change the weight of the composite foams significantly. Our data indicated that AgNWs/polyimide composite foams were ultralightweight, which effectively meet the requirement of lightweight for effective and practical shielding applications.

Table 1. Density and AgNWs Loading of AgNWs/Polyimide Hybrid Composite Foams in the Study

sample	nanowire content in foams (wt %)	nanowire content in foams (vol %)	foam Density (g/cm^3)
PIF-0	0	0	0.014 ± 0.001
PIF-3	1.3	2.02×10^{-3}	0.016 ± 0.001
PIF-5	2.1	3.50×10^{-3}	0.017 ± 0.001
PIF-8	2.7	4.68×10^{-3}	0.018 ± 0.002
PIF-10	3.4	6.22×10^{-3}	0.019 ± 0.001
PIF-13	4.5	7.20×10^{-3}	0.017 ± 0.002
PIF-15	5.5	10.8×10^{-3}	0.021 ± 0.002
PIF-20	7.8	14.8×10^{-3}	0.020 ± 0.002
PIF-13-2	4.5	7.93×10^{-3}	0.018 ± 0.001
PIF-13-3	4.5	8.23×10^{-3}	0.019 ± 0.001
PIF-13-4	4.5	8.78×10^{-3}	0.021 ± 0.002
PIF-13-E	4.5	6.94×10^{-3}	0.016 ± 0.002
PIF-13-S	12.5	22.5×10^{-3}	0.019 ± 0.002
PIF-13-D	20.5	43.9×10^{-3}	0.022 ± 0.002

Figure 3 shows the cell morphology of AgNWs/PI composite foams with different AgNWs loadings. Their apparent viscosity of first solution, average cell diameter, and open cell content are summarized in Table 2. The unloaded PI foams exhibited a uniform microcellular structure with average cell size of 397 μm. The addition of AgNWs decreased the average cell size slightly to 364, 328, and 293 μm for AgNWs loading of 1.3, 2.1, and 2.7 wt %, respectively. With a further increase in AgNWs loading, however, the average cell size tended to increase to 413, 434, 479, and 489 μm for AgNWs loading of 3.4, 4.5, 5.5, and 7.8 wt %, respectively. The observation of the decreasing cell size when nanofillers such as nanoclays,[42] carbon nanofiber,[13] carbon nanotubes,[25] and cellulose nanowhiskers[43] were added to polymer foam systems has been reported previously. This behavior was considered to be ascribed to the effects of nanofillers addition on nucleation and cell growth in the reactive free-rising foaming system.[42−44] In this case, the effects were greater than that in the nonreactive thermoplastic foaming system[45−47] due to the fact that the complex physical and chemical mechanisms occurred simultaneously in reactive foaming system.[48] In our experiment, AgNWs displayed a 2-fold role. On one hand, they acted as nucleating agents and promoted the cell nucleation ascribed to the significant reduction in the required energy for creating cells.[49] On the other hand, they increased the apparent viscosity of first solution (Table 2) because of the formation of AgNWs network via direct contacts by polymer chains.[48,50] Larger amounts of AgNWs promoted the formation of more nucleation sites for cell formation. Meanwhile, the cell growth seemed to be hindered by the increasing viscosity, resulting in a larger number of cells growing to a smaller size. When the AgNWs loading increased to a certain value (3.4 wt %), however, the number of final bubbling nucleation sites tended to be decreased due to the competitive nucleation of too many nucleation sites.[49] At the same time, the higher viscosity of first solution also seemed to hinder the formation of bubbling nucleation due to the decreasing reaction rate between water and isocyanate in the presence of too many rigid AgNWs. As a consequence, the nucleation rate tended to be lower than the cell growth rate, leading to the bigger cell size and inhomogeneous cell distribution. Moreover, the increased pressure inside the small cells ruptured their cell walls, and they coalesced with adjacent large cells to become larger cells.[50−52] It can be seen that the open cell content decreased slightly from 94.6% to 87.6% as the AgNWs loading increased. This indicated that AgNWs did not promote cell opening during cell growth and hence did not cause the loss of blowing gas. This should be ascribed to the fact that the presence of rigid AgNWs lowered polymer chain flexibility and increased the strength of cell films.[51] This highly porous structure also endowed the composite foams with ultralow densities. And the introduction of large volumes of air into the composite foams could limit the mismatch between the wave impedances for the signal propagating in the air and into the shied.[47] Moreover, the presence of microcells created a huge gas−solid interface, which was effective for the multiple reflections of electromagnetic waves.

It has been demonstrated that there is a significant impact of 1D nanofillers aspect ratio (length to diameter ratio, L:D) on the properties of composites.[53−55] Figure 4 shows the effects of AgNWs aspect ratios on the morphology of composite foams in which inset images show the morphology of AgNWs used for each sample. The apparent viscosity of first solution, AgNWs sizes, average cell diameter, and the open cell content are summarized in Table 3. It can be seen that the average cell diameter decreased from 513 to 434 μm with increasing nanowires aspect ratio. Correspondingly, the gas−solid interfacial area tended to increase, and the open cell content (Table 3) decreased slightly from 92.1% to 89.2%. Such a phenomenon also could be explained by the nucleation theory and viscosifying action of AgNWs. For a given nanowire length, increasing the nanowire aspect ratio decreased the nanowire

DOI: 10.1021/am5067095
ACS Appl. Mater. Interfaces 2015, 7, 563−576

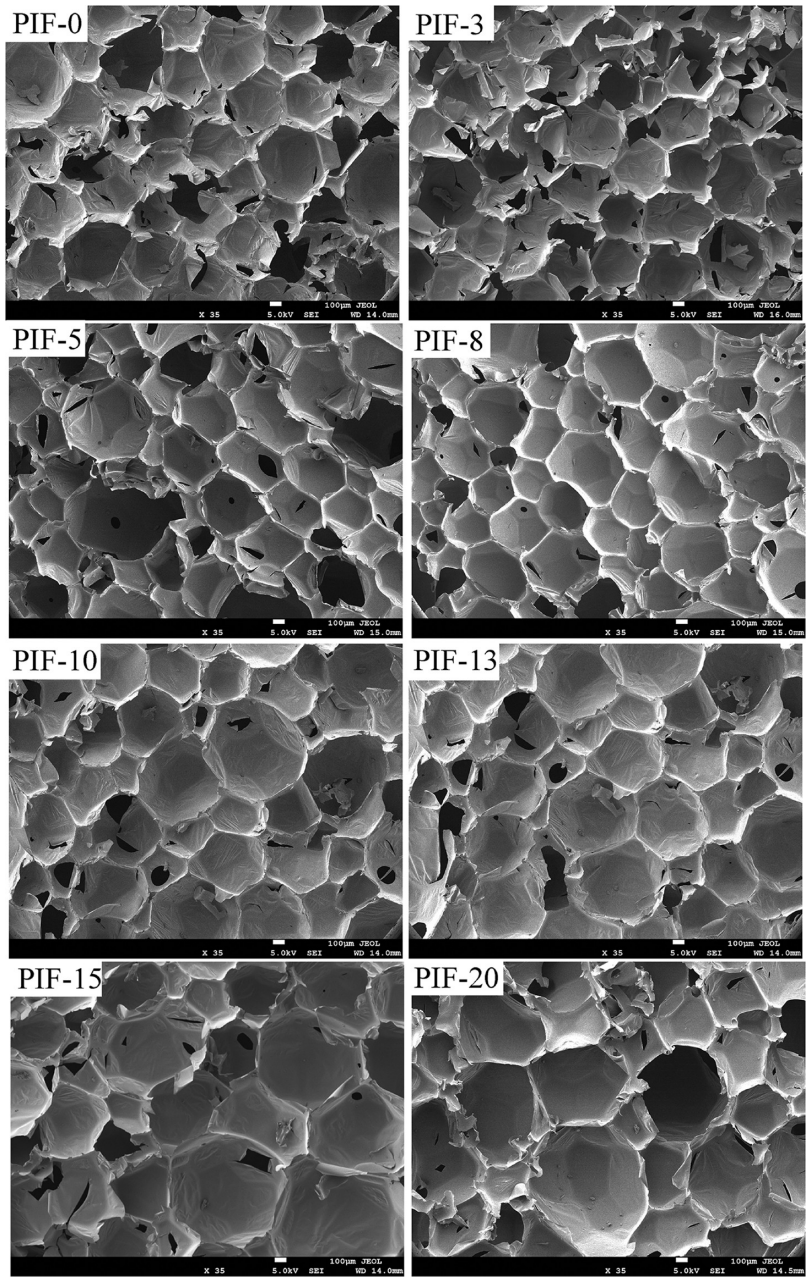

Figure 3. FESEM micrographs of AgNWs/polyimide composite foams as the function of AgNWs content. (PIF-0, 0 wt %; PIF-3, 1.3 wt %; PIF-5, 2.1 wt %; PIF-8, 2.7 wt %; PIF-10, 3.4 wt %; PIF-13, 4.5 wt %; PIF-15, 5.5 wt %; PIF-20, 7.8 wt %).

Table 2. Morphological Properties of AgNWs/Polyimide Hybrid Composite Foams as the Function of AgNWs Content

AgNWs content (wt %)	0	1.3	2.1	2.7	3.4	4.5	5.5	7.8
apparent viscosity (mPa·s)	489	624	738	986	1021	1050	1088	1100
maximum cell size (μm)	631	489	589	452	697	655	794	841
minimum cell size (μm)	273	244	143	168	256	255	278	326
average Cell diameter (μm)	397 ± 86	364 ± 94	328 ± 102	293 ± 78	413 ± 99	434 ± 106	479 ± 119	489 ± 135
open cell content (%)	94.6 ± 0.8	94.0 ± 0.4	93.3 ± 0.2	92.8 ± 0.4	90.4 ± 0.3	89.2 ± 0.3	88.1 ± 0.2	87.6 ± 0.5

diameter, leading to the increase in the number of AgNWs. Thus, a larger number of cells began to nucleate, resulting in smaller cells. Meanwhile, the increasing apparent viscosity (Table 3) could limit the cell expansion and lead to a reduction in cell size and open cell content. It was also found that the cell size displayed a broad distribution, possibly ascribed to the coalescence effects during the cell growth at this nanowire loading.

3.1.2. Distribution of AgNWs in Cell Walls. The distribution of AgNWs in cell structure was investigated by FESEM, and the results are displayed in Figure 5. As indicated in Figure 5a, with magnification of 1000×, cell walls of adjacent microcells created triangular cell conjunctions. A higher magnification (Figure 5b)

DOI: 10.1021/am5067095
ACS Appl. Mater. Interfaces 2015, 7, 563−576

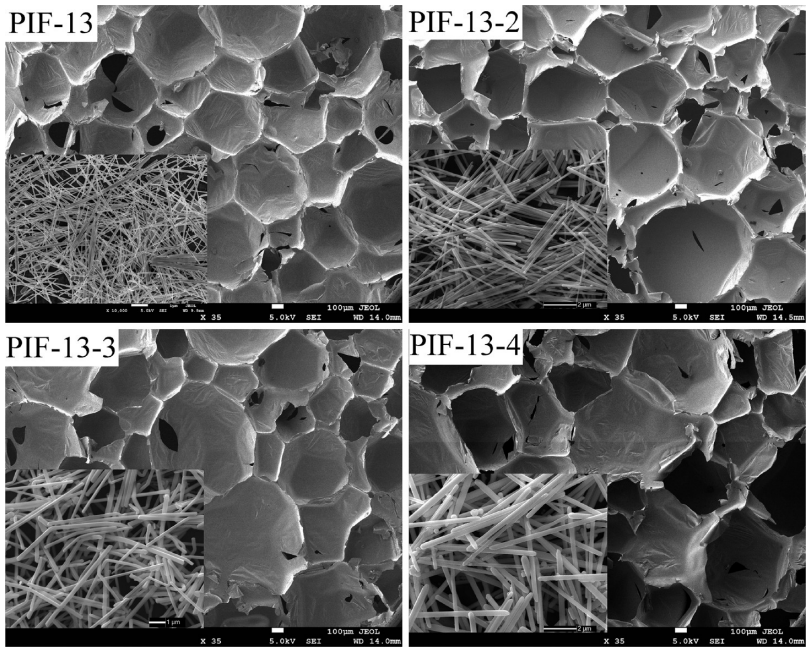

Figure 4. FESEM micrographs of AgNWs/polyimide composite foams as the function of nanowires aspect ratio (PIF-13, R = 79; PIF-13-2, R = 47; PIF-13-3, R = 34; PIF-13-4, R = 25). Inset shows the morphology of AgNWs used for each sample.

Table 3. Morphological Properties of AgNWs/Polyimide Hybrid Composite Foams as the Function of AgNWs Aspect Ratio

sample	PIF-13	PIF-13-2	PIF-13-3	PIF-13-4
AgNWs aspect ratio	79	47	34	25
diameter of wires (nm)	90 ± 21	156 ± 35	225 ± 28	285 ± 42
length of wires (μm)	7.1 ± 2.5	7.4 ± 1.8	7.6 ± 3.2	7.2 ± 2.1
apparent viscosity (mPa·s)	924	886	796	708
maximum cell size (μm)	655	810	806	815
minimum cell size (μm)	255	290	267	280
average cell diameter (μm)	434 ± 106	462 ± 128	486 ± 94	513 ± 138
open cell content (%)	89.2 ± 0.3	91.3 ± 0.2	91.6 ± 0.2	92.1 ± 0.3

shows the clear distribution of AgNWs in the composite foams, being mainly dispersed in the struts and walls of the cellular structure. Although trace amounts of AgNWs were distributed in the ultrathin cell membranes. It can be observed that the AgNWs oriented along the cell walls, possibly due to the strong stretching flow generated during the cell growth. Moreover, a large number of AgNWs were coated with polymer resin. Figure 5c presents a single nanowire standing out from the cell walls, indicating that the AgNWs with diameter of 90 nm were also located in normal direction of cell walls. According to the FESEM micrographs, we suggest that interconnected AgNWs networks structure was formed in the cell walls and struts, shown in Figure 5d. In consideration of the 3D interconnected network structure of PIF, a large 3D AgNWs network also existed in the whole foam, which would play an important part in improving the EMI shielding performance.

To further observe the distribution of AgNWs in composite foams, PIF-8, PIF-13, and PIF-20 were selected to be subjected to chemical etching so that the polymer resin coated on the AgNWs was etched. A low magnification FESEM image of PIF-13 after etching is shown in Figure 6a. It can be seen that the cell membranes were almost broken, leading to some collapsed cells. At higher magnification (Figure 6b), it is possible to view several bright areas in the cell walls that appeared to be the dispersed AgNWs. The inset picture shows the microcosmic morphology of the bright areas. It can be clearly observed that the exposed AgNWs were deposited uniformly and densely on the unbroken cell walls, and they intertwined with each other. Combined with the 3D AgNWs networks created by 3D structure of foams, the interconnected AgNWs networks in cell walls provided fast electron transport channels inside foams, which would be effective for electromagnetic waves attenuation. Therefore, such ultralightweight AgNWs/polyimide composite foams are expected to display a high EMI shielding performance.

The morphologies of foams at different AgNWs loadings after etching are shown in Figure 7. At AgNWs loading of 2.7 wt %, the AgNWs in polyimide matrix were sparse and their distribution was uniform. However, the amount of connections between AgNWs was quite small, which was unfavorable for improving EMI shielding performance significantly (Figure 7a1,a2). At higher AgNWs loading of 4.2 wt %, the AgNWs were densely distributed in cell walls and intertwined with each other to form a 3D network. In this case, a large number of connections between AgNWs tended to improve EMI shielding performance, as indicated in Figure 7b1,b2. With a further increase to 7.8 wt % in AgNWs loading, a larger amount of AgNWs was densely dispersed in the matrix and constructed denser 3D networks. More importantly, in addition to the interconnected networks between AgNWs, many of the AgNWs formed segregated nanowires networks resembling a cell-like structure, which would play a critical role in further

DOI: 10.1021/am5067095
ACS Appl. Mater. Interfaces 2015, 7, 563−576

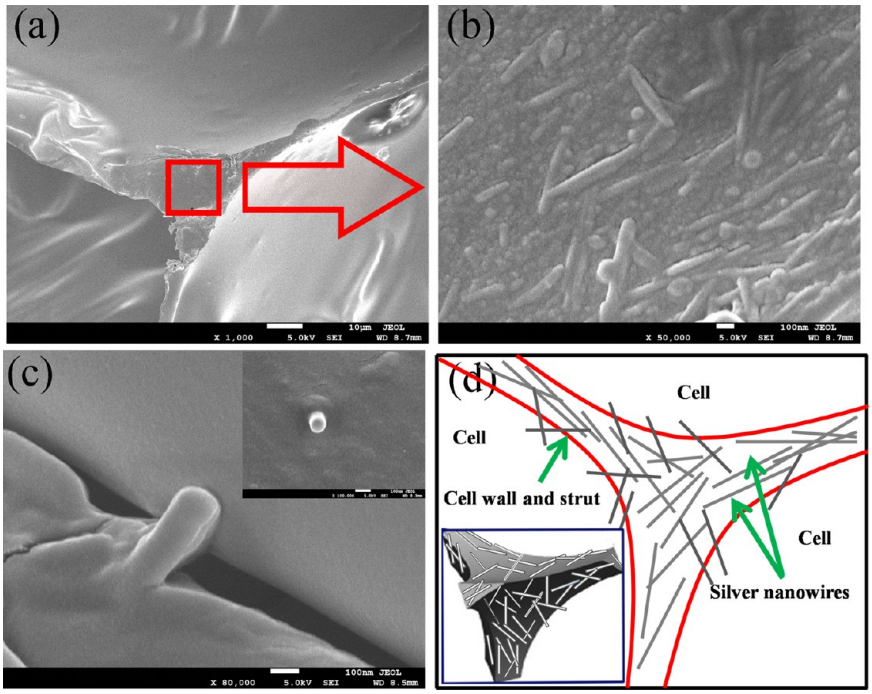

Figure 5. Dispersion of AgNWs in composite foams: (a) FESEM image of cell walls, (b) FESEM image of the distribution of AgNWs in cell walls at high magnification. (c) Side view of a single nanowire in cell wall, inset shows the elevation view of a single nanowires. (d) Schematic model of the distribution of AgNWs in composite foams, inset shows the 3D model of the distribution of AgNWs in composite foams.

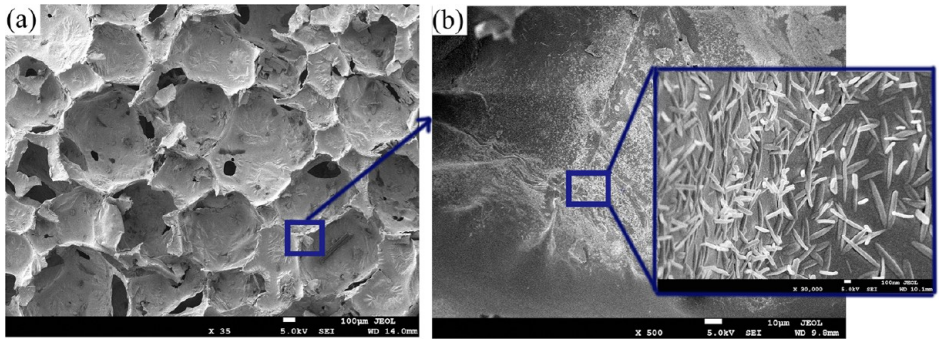

Figure 6. (a) FESEM images of cell morphology of PIF-13 after etching. (b) FESEM image of cell wall morphology after etching, inset picture shows the morphology of AgNWs exposed on the cell walls.

improving EMI shielding performance (Figure 7c1,c2). Our data suggested that increasing the AgNWs loading increased the number of connections between the nanowires in the cell walls, thereby increasing the conductivity of networks. As a result, such ultralightweight AgNWs/polyimide composites are an ideal material for blocking the unwanted electromagnetic waves because of the presence of highly interconnected conductive networks.

3.1.3. Morphology of AgNWs/PI Composite Foams Coated with AgNWs. It has been found that surface metallization by depositing or spraying for polymer composites is an effective approach to enhance the EMI SE of shielding materials.[56−58] Two PIF-13 samples were selected to spray AgNWs on their surfaces. Microstructures of the AgNWs-coated composite foam surface were analyzed by an FESEM coupled with an EDS (Figure 8). As shown in Figure 8a,b, the surface was completely covered with AgNWs after spraying. It was found that the open cell content decreased to 87.5%−85.8%, possibly due to the fact that the surface cells were blocked by the AgNWs coated on the surface. Figure 8c displays the structure of the dispersed AgNWs on the surface. It is worth noting that AgNWs connected with each other to generate a dense and seamless 2D network. Figure 8d shows the EDS of AgNWs coated composite foam surface. The EDS at the cell membranes indicated that the major element on the spraying surface was Ag due to the appearance of strong peaks at about 3 keV. The elements C and O should stem from the substances underneath the depositional silver, and the Pt came from the spaying Pt in the testing process. In this case, the seamlessly interconnected 2D AgNWs networks throughout the surface would establish fast electrical conduction pathways, which would be critical and leaded to further improved EMI shielding performance.

To investigate the immersion depth and interfacial bonding of coated AgNWs in composite foams, the cross-sectional structure of AgNWs-coated composite foam was examined. Figure 9a displays the FESEM cross-sectional image of the AgNWs-coated composite foam in which Part I, Part II, and Part III are the regions about 0.35, 0.6, and 1.1 mm from the outside surface. It can be noticed that the AgNWs networks gradually disappeared from Part I to Part III, as indicated in

DOI: 10.1021/am5067095
ACS Appl. Mater. Interfaces 2015, 7, 563−576

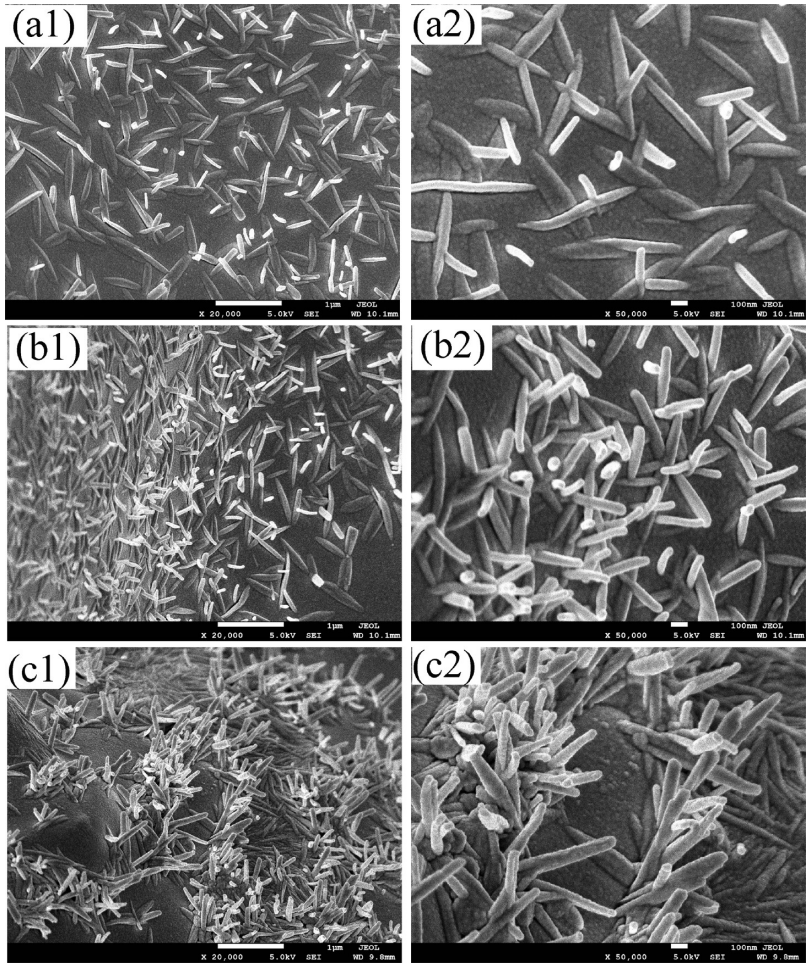

Figure 7. FESEM images of the distribution of AgNWs in composite foams after etching: a1, a2, PIF-8; b1, b2, PIF-13; c1, c2, PIF-20.

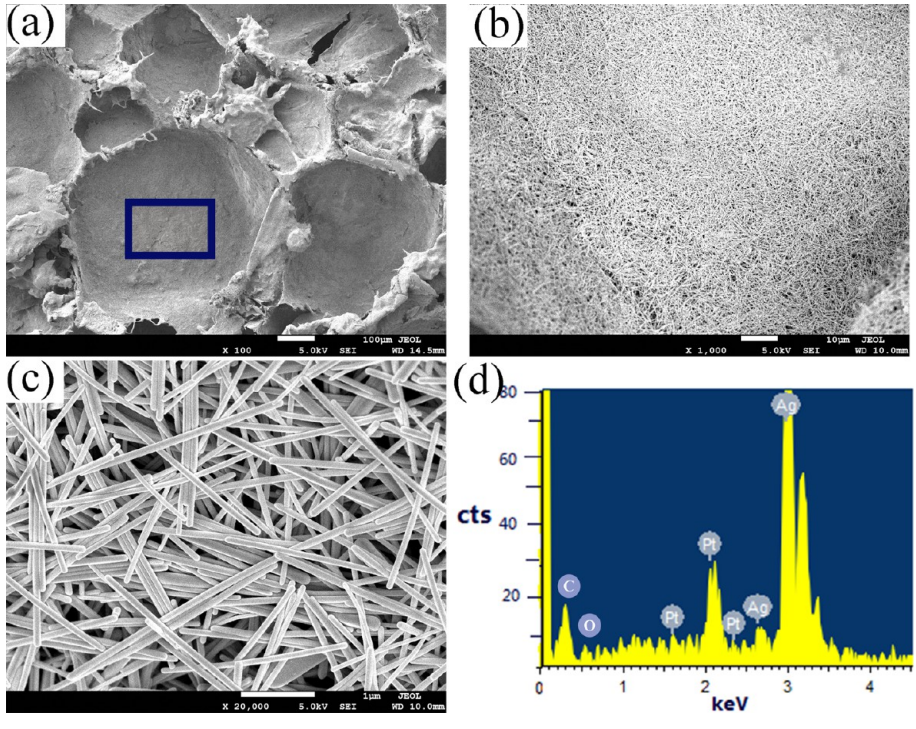

Figure 8. (a) FESEM image of AgNWs-coated composite foam surface. (b) Morphology of silver AgNWs-coated nanocomposite foam surface at high magnification. (c) Morphology of the AgNWs coated on the surface. (d) EDS spectrum of AgNWs-coated composite foam surface.

DOI: 10.1021/am5067095
ACS Appl. Mater. Interfaces 2015, 7, 563−576

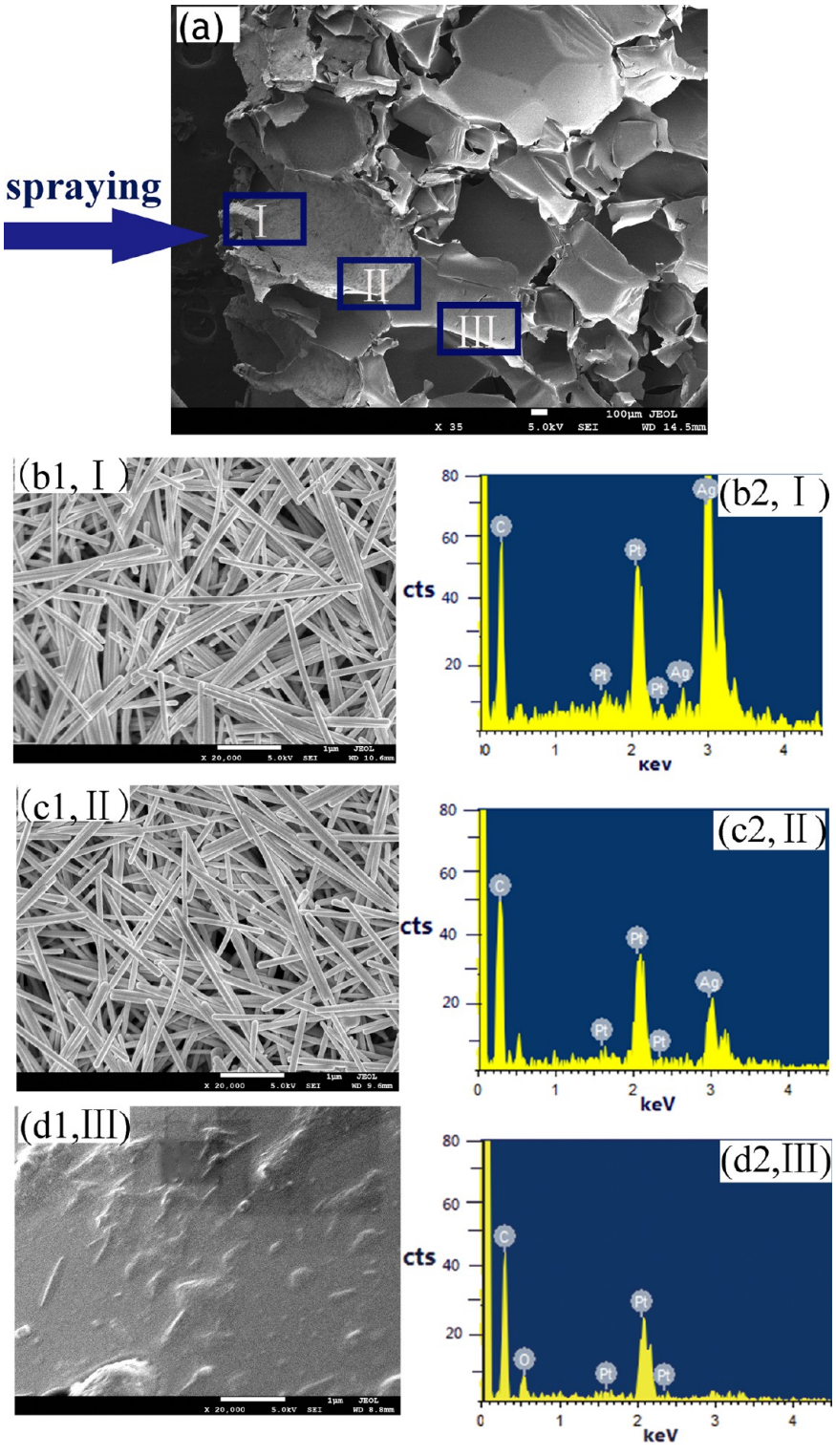

Figure 9. (a) FESEM image of the profile of coated composite foam; FESEM images of the structure for Part I (b1), Part II (c1), and Part III (d1) at high magnification. EDS spectrum of coated composite foam in Part I (b2), Part II (c2), and Part III (d2).

FESEM micrographs with higher magnification of the three regions (Figure 9b1–d1). Figure 9(b2–d2) presents typical EDS images of the three regions. It is important to note that Part I, Part II, and Part III were characterized by decreasing silver proportions from exterior to interior surface, which was consist with the results of FESEM images. The sprayed AgNWs were mainly dispersed on the surface layer in 460 μm depth and tightly bound to the polymer matrix due to the van der Waals force and Coulomb force.[58] Our data indicated that AgNWs had a good interfacial bonding with the composite foam matrix.

3.2. EMI Shielding Performance of AgNWs/Polyimide Composite Foams. EMI SE is used to evaluate the material's ability to attenuate the electromagnetic wave strength and is expressed in dB. It is defined as the logarithmic ratio of incoming power (P_i) to transmitted power (P_t) of an electromagnetic wave. The total SE consists of reflection loss

DOI: 10.1021/am5067095
ACS Appl. Mater. Interfaces 2015, 7, 563–576

(SE_R), absorption loss (SE_A), and multiple reflection loss (SE_M) as shown in eq 1.[8,59,60] The higher the dB level of EMI SE, the more electromagnetic incident waves are blocked by the shielding material.

$$SE = 10\lg \frac{P_i}{P_t} = SE_R + SE_A + SE_M \quad (1)$$

It is well-known that the reflection loss results from the mismatch of the intrinsic impedance between the shield and the air, the absorption loss results from the dissipative energy absorption of microwaves in the shield, and the multiple-reflection loss results from the internal nonuniformity of the shielding materials.[8] For plane wave radiation, SE_R and SE_A may also be calculated from the following equations:[60,61]

$$SE_A = 20\lg e^{t/\delta} = 8.68t/\delta = 8.68t\sqrt{\pi\mu\sigma f} \quad (2)$$

$$SE_R = 20\lg\left(\frac{\eta_0}{4\sqrt{2\pi f\mu/\sigma}}\right) \quad (3)$$

where t is the shield thickness, δ is the skin depth, σ is the electrical conductivity, f is the frequency of electromagnetic wave, μ is the magnetic permeability of the shield, η_0 is the impendence of free space ($\eta_0 = 120\Pi = 377\ \Omega$). However, the equations above are used for conductive monolithic materials, and they are not completely suitable for shielding material with a composite foam structure. Nevertheless, it is desirable to anticipate the general effects of different parameters on the EMI SE in such composite foams using these two equations as criterions. It is evident that the absorption loss increases with increasing thickness, conductivity and frequency, while the reflection loss increases with increasing conductivity and decreases with increasing frequency.

Figure 10a shows the EMI SE of AgNWs/PI composite foams with different AgNWs loadings measured in the frequency ranges of 30 MHz−1.5 GHz. A pure PIF without AgNWs was obviously transparent to electromagnetic waves and exhibited almost no shielding ability. The addition of AgNWs could improve the EMI SE effectively. The EMI SE of all samples was found to decrease with increasing frequency from 30 to 800 MHz. With a further increase in frequency, the EMI SE reached a plateau. For instance, for a given nanowires loading like 7.8 wt %, the EMI SE decreased from 21 dB at 200 MHz to 9 dB at 1000 MHz, as shown in Figure 10b. It is well-known that reflection loss is the dominant contribution to EMI shielding at low frequency, while the shielding mechanisms are reflection loss and absorption loss at high frequency. According to eq 3, the changes above emerged. It is notable that the SE increased continuously with increasing AgNWs content at the same frequency, possibly due to the variation in densities of interconnected AgNWs networks distributed in the foams. Figure 10b clearly shows the increasing trend. For instance, the EMI SE increased from 12 to 21 dB at 200 MHz, from 3 to 11 dB at 600 MHz, and from 1.5 to 9 dB at 1000 MHz with increasing nanowires loading from 1.3 to 8.2 wt %. It has been noted that increasing AgNWs loading increased the number of connections between the nanowires in cell walls, thereby increasing conductivity of nanowires networks. As given by eqs 2 and 3, the EMI SE increased gradually. In particular, the specific EMI SE is a more appropriate criterion to compare the shielding performance between the AgNWs/polyimide composite foams and other materials for applications that need

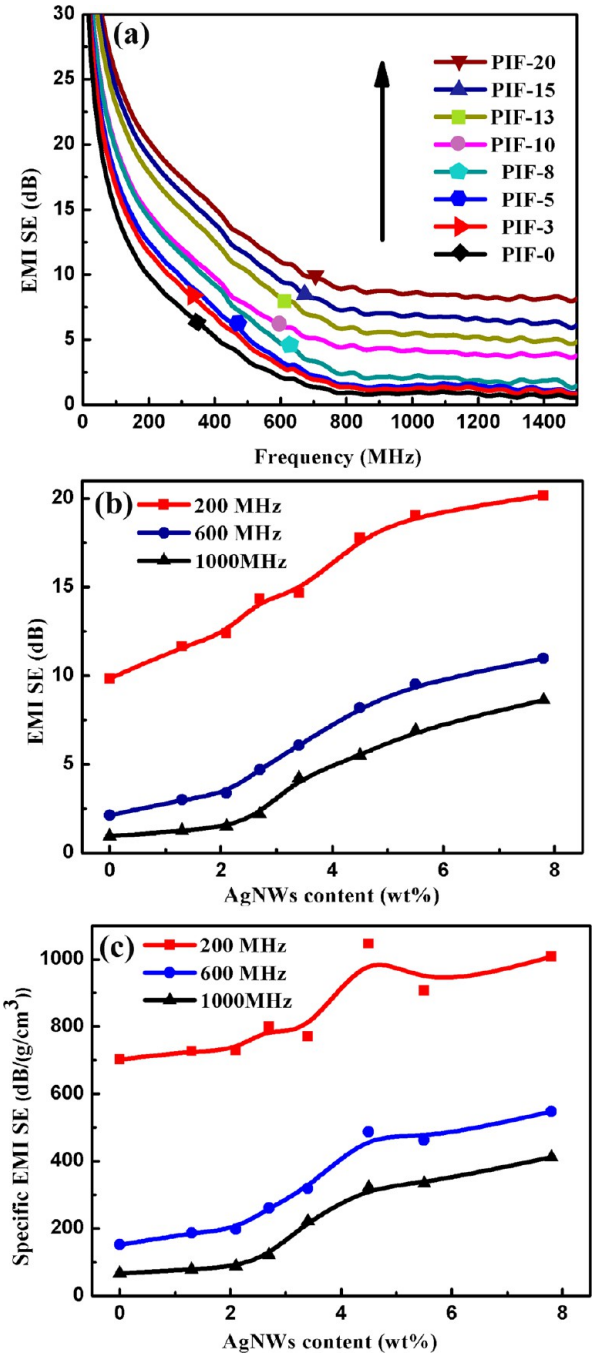

Figure 10. (a) EMI SE of AgNWs/polyimide composite foam in different nanowire contents with respect to the frequency. (b) EMI SE and (c) specific EMI SE of AgNWs/PI nanocomposite foam with respect to nanowires content at 200, 600, and 1000 MHz.

lightweight materials. As shown in Figure 10c, the specific SE of the composite foams with 8.1 wt % AgNWs was 1008 $dB{\cdot}g^{-1}{\cdot}cm^3$ at 200 MHz, 557 $dB{\cdot}g^{-1}{\cdot}cm^3$ at 600 MHz, and 412 $dB{\cdot}g^{-1}{\cdot}cm^3$ in the frequency range of 800−1500 MHz. Our data indicated that the good SE combined with ultralow density endowed the AgNWs/polyimide composite foam with a superior specific EMI SE, which is very desirable for applications that need lightweight materials such as computer devices.

It was found that nanowire aspect ratio had impact on the conductivity of nanowire film.[62] In this part, we addressed the

DOI: 10.1021/am5067095
ACS Appl. Mater. Interfaces 2015, 7, 563−576

AgNWs aspect ratio as the variation factor to demonstrate its effect on the EMI SE of composite foams. The EMI SE of samples with various nanowire aspect ratios were measured at 30 MHz−1.5 GHz and the results were displayed in Figure 11a.

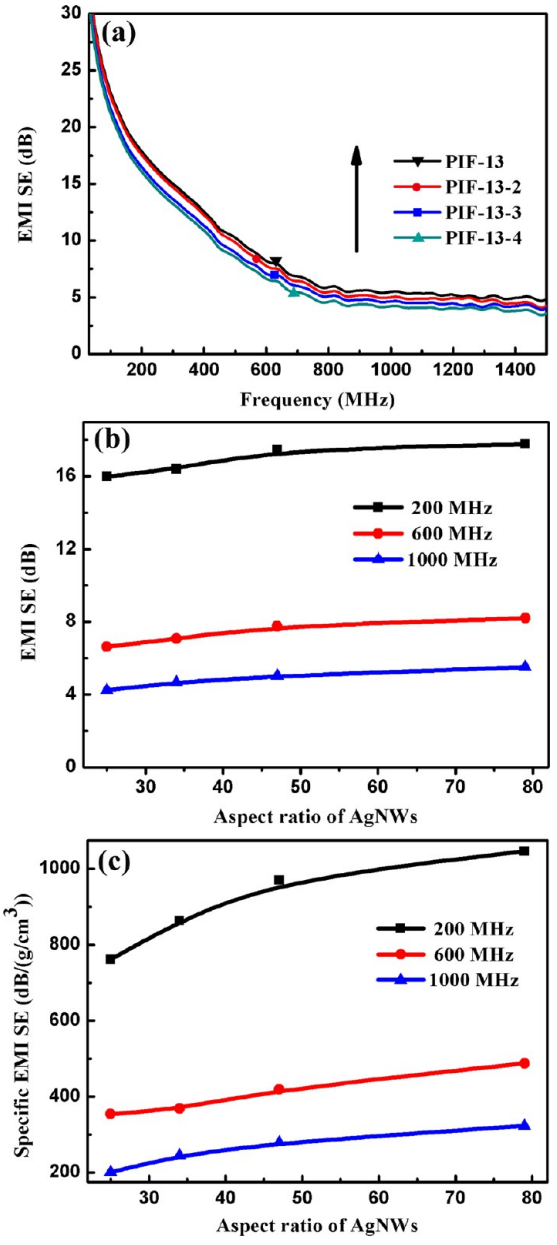

Figure 11. (a) EMI SE of AgNWs/polyimide composite foam in different nanowire aspect ratios with respect to the frequency. (b) EMI SE and (c) specific EMI SE of AgNWs/polyimide composite foam with respect to nanowires aspect ratio at 200, 600, and 1000 MHz.

The EMI SE and specific EMI SE as the function of nanowire aspect ratio at 200, 600, and 1000 MHz are presented in Figure 11b,c, respectively. It can be seen that the SE increased slightly with increasing nanowire aspect ratio at the same frequency. This could be due to the slight differences in the connections between the nanowires. It is believed that, for a given weight and nanowire length, increasing aspect ratio increased the number of connections between the nanowires. Increasing the number of connections increased the conductivity of the nanowire network, and, as given by eqs 2 and 3, increased the EMI SE for composite foams. Moreover, the increasing interface area with the aspect ratio might also contribute to the enhancement of the EMI SE. However, this increasing trend was very slow. For instance, the EMI SE for composite foams at a nanowire aspect ratio of 79 was only about 2 dB higher than that for composite foams at a nanowires aspect ratio of 27. The results demonstrated that AgNWs with a low aspect ratio have already intertwined with each other to form a conduction network with a 4.5 wt % loading. For networks where the AgNWs are highly connected, nanowires with smaller diameters would outperform nanowires with larger diameters. In view of the above, a lower loading of nanofillers might be enough to achieve effective EMI shielding performance for AgNWs with higher aspect ratio.

It is well-known that the conduction networks constructed on the surface can enhance the EMI SE of shielding materials significantly.[8] In this part, we focus on the EMI SE of composite foams after surface etching or spraying in the frequency of 30−1500 MHz, as shown in Figure 12. The

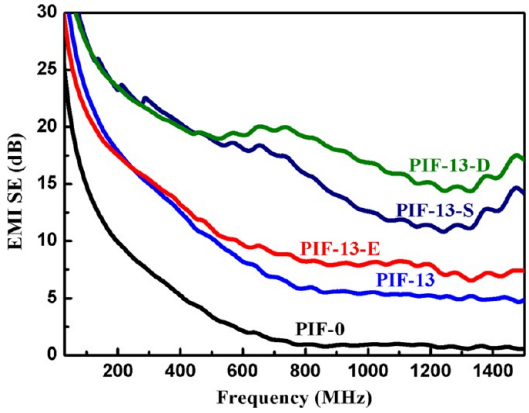

Figure 12. EMI SE of AgNWs/polyimide composite foams before and after etching or spraying with respect to the frequency. (PIF-13, without etching or spraying; PIF-13-E, after etching; PIF-13-S, after spraying with one surface; PIF-13-D, after spraying with two surfaces).

corresponding EMI SE and specific EMI SE for samples at 200, 600, and 1000 MHz are summarized in Table 4. It is worth noting that the EMI SE of composite foam (PIF-13-E) was enhanced after etching. For instance, the EMI SE increased from 8.2 to 10 dB at 600 MHz, and from 5.4 to 8 dB at 1000 MHz. It is evident that surface etching facilitated the building of shielding networks on the surface due to the showing up of the AgNWs buried in polymer resin, which would reflect the electromagnetic wave effectively. More importantly, the EMI SE was improved more significantly after spraying samples with AgNWs (PIF-13-S, PIF-13-D). This could be due to the existence of seamlessly interconnected AgNWs networks on the surface. Specially, the EMI SE of the foam with two surface sprayed with AgNWs (PIF-13-D) was higher than that of the foam with one surface sprayed especially at high frequencies. This may be ascribed to the thicker shielding networks which could reflect the remaining waves propagating to another surface. It is well established that depositing an AgNWs film with excellent electrical conductivity on the surface of the composite foams (shown in Figure 8) added a seamlessly interconnected AgNWs network. We suggested that both reflections resulting from the AgNWs networks on the foam surface and inside cell walls contributed to the shielding effect,

DOI: 10.1021/am5067095
ACS Appl. Mater. Interfaces 2015, 7, 563−576

Table 4. EMI SE and Specific EMI SE of Composite Foams for PIF-0, PIF-13, PIF-13-E, PIF-13-S, and PIF-13-D at 200, 600, and 1000 MHz

samples		PIF-0	PIF-13	PIF-13-E	PIF-13-S	PIF-13-D
EMI SE (dB)	200 MHz	9	18	18	23	23.5
	600 MHz	2	8.2	10	18	19.3
	1000 MHz	1	5.4	8	12.6	17
specific EMI SE ($dB \cdot g^{-1} \cdot cm^3$)	200 MHz	642	1058	1125	1210	1068
	600 MHz	142	487	586	957	856
	1000 MHz	71	318	471	663	772

but the reflection of AgNWs networks on the foam surface was the dominant mechanism. Our data demonstrated that appropriate surface treatments like etching or spraying increased the density of AgNWs networks on the surface, and increased the conductivity of networks, thereby improving the EMI shielding performance. In particular, the maximum specific SE values of 1210 $dB \cdot g^{-1} \cdot cm^3$ for PIF-13-S (0.023 vol % AgNWs loading) at 200 MHz, 957 $dB \cdot g^{-1} \cdot cm^3$ for PIF-13-S at 600 MHz and 772 $dB \cdot g^{-1} \cdot cm^3$ for PIF-13-D (0.044 vol % AgNWs loading) at 800−1500 MHz were achieved, respectively. These values are much higher than those of typical shielding materials at the same frequency range previously reported in the literature. For instance, 15 $dB \cdot g^{-1} \cdot cm^3$ for polyethylene−carbon fiber composites with 20 wt % (11 vol %) carbon fiber loading,[63] 35.3 $dB \cdot g^{-1} \cdot cm^3$ for reduced graphene oxide (rGO)/epoxy composites containing 2 wt % rGO,[64] and 500 $dB \cdot g^{-1} \cdot cm^3$ graphene/polydimethylsiloxane (PDMS) foams with 0.8 wt % (about 0.037 vol %) graphene loading[65] were achieved at 30 MHz ∼ 1.5 GHz, respectively. Our data indicated that AgNWs-based polymer composites exhibited superior specific EMI SE to the carbon-based polymer composites. This is considered to be due to the 1D AgNWs having superior electrical conductivity and the interconnected AgNWs network providing a fast electron transport pathway. The superior EMI SE allows the use of AgNWs/polyimide composite foam in the areas that need lightweight materials.

We also analyzed the EMI shielding mechanism of AgNWs/polyimide composite foams in this work. According to eqs 1, 2, and 3, for conductors with high electrical conductivity, such as Ag, the main electromagnetic shielding mechanisms are reflection loss and absorption loss. Because of the limit of the measurement equipment, we could not calculate the SE_R and SE_A for composite foams in the 30 MHz−1.5 GHz frequency range. However, on the basis of the results reported above, we suggest that reflection loss is the major contribution to EMI shielding in the AgNWs/PI composite foams at low frequency, whereas the EMI shielding mechanisms are reflection loss and absorption loss at high frequency. According to eqs 1, 2, and 3, we can notice that $SE_R \propto \lg \sigma$ and $SE_A \propto \sigma^{0.5}$. The interconnected AgNWs network in the cell walls combined with the 3D AgNWs network formed by copying the structure of the whole foam could provide fast electronic channels inside the foam, thereby increasing the conductivity. Consequently, the AgNWs/PI composite foams are both reflective and absorptive to electromagnetic waves. Furthermore, multiple reflections resulting from the reflection at various interfaces inside the shield could be another shielding mechanism that was influenced by the porous structure. The presence of cells created a huge gaseous cell−polymer matrix interface area. And the large aspect ratio of AgNWs also induced a large AgNWs−polymer resin interface area. The incident electromagnetic waves would be repeatedly reflected and scattered at these interfaces numerous times. The multiple reflections make it difficult for the electromagnetic waves to escape from the foam before being dissipated as heat. Moreover, appropriate surface treatment like etching or spraying facilitated the construction of seamlessly interconnected 2D AgNWs networks on the surface, which could reflect electromagnetic waves more effectively. In brief, the reflections of interconnected AgNWs networks on the surface and inside the shield combined with the multiple reflections at interfaces inside the shield contributed to the shielding effect.

4. CONCLUSION

(1) In summary, we have developed a fast, facile, and scalable approach to fabricate ultralightweight AgNWs hybrid polyimide composite foams for high-performance EMI shielding using a one-pot liquid foaming process. The morphology and the EMI SE at 30 MHz−1.5 GHz of AgNWs/polyimide composite foams at various AgNWs loadings or AgNWs aspect ratios, composite foams subjected to etching, and composite foams sprayed with AgNWs were studied.

(2) The as-prepared foams exhibited low densities of 0.014−0.022 g/cm^3 and microcellular structure with average diameter of 293−513.4 μm. And the open cell content was found to be 94.6%−85.8%. The interconnected AgNWs networks throughout cell walls combined with the 3D AgNWs networks created by a 3D structure of foams provided fast electron transport channels inside foams, which is effective for electromagnetic waves attenuation.

(3) The EMI SE of these foams increased with increasing AgNWs content as well as the aspect ratio due to the increasing number of connections between AgNWs. And the foam with 7.8 wt % (0.015 vol %) loading displayed a high EMI SE of 30−9 dB over a frequency range of 30 MHz−1.5 GHz. Appropriate surface treatment like etching or spraying facilitated the construction of interconnected 2D AgNWs networks on the surface, which could effectively reflect electromagnetic waves. The AgNWs coated on the surface which functioned as an enhanced coating, were tightly bound to the polymer matrix in 460 μm depth and constructed denser 2D shielding networks. This caused a maximum EMI SE of 45−16 dB at 30 MHz−1.5 GHz. More importantly, its specific EMI SE could reach 1210 $dB \cdot g^{-1} \cdot cm^3$ at 200 MHz, 957 $dB \cdot g^{-1} \cdot cm^3$ at 600 MHz, and 772 $dB \cdot g^{-1} \cdot cm^3$ at 800−1500 MHz containing <0.044 vol % AgNWs loading, which far surpasses the best values of other composite materials.

(4) The reflections of interconnected AgNWs networks on the surface and inside the shield combined with the multiple reflections at gas−solid interfaces and AgNWs−resin interfaces contributed to the shielding effect.

The fabrication of this novel material opens up the possibility for the use of AgNWs/polyimide composite foams as a lightweight, and high-performance EMI shielding material for

DOI: 10.1021/am5067095
ACS Appl. Mater. Interfaces 2015, 7, 563−576

applications in the civil fields such as electronics, computers, and so on.

AUTHOR INFORMATION

Corresponding Author

*M. Zhan. E-mail: zhanms@buaa.edu.cn. Tel: +86 10 82338557.

Author Contributions

The paper was written through contributions of all authors. All authors have given approval to the final version of the paper.

Notes

The authors declare no competing financial interest.

REFERENCES

(1) Shen, B.; Zhai, W. T.; Zheng, W. G. Ultrathin Flexible Graphene Film: An Excellent Thermal Conducting Material with Efficient EMI Shielding. *Adv. Funct. Mater.* **2014**, *24*, 4542−4548.

(2) Song, W. L.; Wang, J.; Fan, L. Z.; Li, Y.; Wang, C. Y.; Cao, M. S. Interfacial Engineering of Carbon Nanofiber−Graphene−Carbon Nanofiber Heterojunctions in Flexible Lightweight Electromagnetic Shielding Networks. *ACS Appl. Mater. Interfaces* **2014**, *6*, 10516−10523.

(3) Chen, M.; Zhang, L.; Duan, S.; Jing, S.; Jiang, H.; Luo, M.; Li, C. Highly Conductive and Flexible Polymer Composites with Improved Mechanical and Electromagnetic Interference Shielding Performances. *Nanoscale* **2014**, *6*, 3796−3803.

(4) Maiti, S.; Shrivastava, N. K.; Suin, S.; Khatua, B. B. Polystyrene/MWCNT/Graphite Nanoplate Nanocomposites: Efficient Electromagnetic Interference Shielding Material through Graphite Nanoplate-MWCNT-Graphie Nanoplate Networking. *ACS Appl. Mater. Interfaces* **2013**, *5*, 4712−4724.

(5) Fletcher, A.; Gupta, M. C.; Dudley, K. L.; Vedeler, E. Elastomer Foam Nanocomposites for Electromagnetic Dissipation and Shielding Applications. *Compos. Sci. Technol.* **2010**, *70*, 953−958.

(6) Eswaraiah, V.; Sankaranarayanan, V.; Ramaprabhu, S. Functionalized Graphene−PVDF Foam Composites for EMI Shielding. *Macromol. Mater. Eng.* **2011**, *296*, 894−898.

(7) Fletcher, A.; Gupta, M. C. Mechanical Properties of Elastomer Nanocomposites for Electromagnetic Interference Shielding Applications. *J. Compos. Mater.* **2014**, *48*, 1261−1276.

(8) Ji, K. J.; Zhao, H. H.; Zhang, J.; Chen, J.; Dai, Z. D. Fabrication and Electromagnetic Interference Shielding Performance of Open-Cell Foam of a Cu−Ni Alloy Integrated with CNTs. *Appl. Surf. Sci.* **2014**, *311*, 351−356.

(9) Ji, K. J.; Zhao, H. H.; Huang, Z. G.; Dai, Z. D. Performance of Open-Cell Foam of Cu−Ni Alloy Integrated with Graphene as a Shield against Electromagnetic Interference. *Mater. Lett.* **2014**, *122*, 244−247.

(10) Micheli, D.; Morles, R. B.; Marchetti, M.; Moglie, F.; Primiani, V. M. Broadband Electromagnetic Characterization of Carbon Foam to Metal Contact. *Carbon* **2014**, *68*, 149−158.

(11) Kumar, R.; Dhakate, S. R.; Saini, P.; Mathur, R. B. Improved Electromagnetic Interference Shielding Effectiveness of Light Weight Carbon Foam by Ferrocene Accumulation. *RSC Adv.* **2013**, *3*, 4145−4151.

(12) Antunes, M.; Velasco, J. I. Multifunctional Polymer Foams with Carbon Nanoparticles. *Prog. Polym. Sci.* **2014**, *39*, 486−509.

(13) Harikrishnan, G.; Singh, S. N.; Kiesel, E.; Macosko, C. W. Nanodispersions of Carbon Nanofiber for Polyurethane Foaming. *Polymer* **2010**, *51*, 3349−3353.

(14) Thomassin, J. M.; Vuluga, D.; Alexandre, M.; Jérôme, C.; Molenberg, I.; Huynen, I.; Detrembleu, C. A Convenient Route for the Dispersion of Carbon Nanotubes in Polymers: Application to the Preparation of Electromagnetic Interference (EMI) Absorbers. *Polymer* **2012**, *53*, 169−174.

(15) Al-Saleh, M. H.; Saadeh, W. H.; Sundararaj, U. EMI Shielding Effectiveness of Carbon Based Nanostructured Polymeric Materials: A Comparative Study. *Carbon* **2013**, *60*, 146−156.

(16) Chen, D.; Miao, Y.; Liu, T. X. Electrically Conductive Polyaniline/Polyimide Nanofiber Membranes Prepared via a Combination of Electrospinning and Subsequent in Situ Polymerization Growth. *ACS Appl. Mater. Interfaces* **2013**, *5*, 1206−1212.

(17) Yang, Y.; Gupta, M. C.; Dudley, K. L.; Lawrence, R. W. Conductive Carbon Nanofiber−Polymer Foam Structures. *Adv. Mater.* **2005**, *17*, 1999−2003.

(18) Yang, Y.; Gupta, M. C. Novel Carbon Nanotube-Polystyrene Foam Composites for Electromagnetic Interference Shielding. *Nano Lett.* **2005**, *5*, 2131−2134.

(19) Yan, D. X.; Ren, P. G.; Pang, H.; Fu, Q.; Yang, M. B.; Li, Z. M. Efficient Electromagnetic Interference Shielding of Lightweight Graphene/Polystyrene Composite. *J. Mater. Chem.* **2012**, *22*, 18772−18774.

(20) Zhang, H. B.; Yan, Q.; Zheng, W. G.; He, Z.; Yu, Z. Z. Tough Graphene-Polymer Microcellular Foams for Electromagnetic Interference Shielding. *ACS Appl. Mater. Interfaces* **2011**, *3*, 918−924.

(21) Ling, J. Q.; Zhai, W. T.; Feng, W.; Zhang, J. F.; Zheng, W. G. Facile Preparation of Light Weight Microcellular Polyetherimide/Graphene Composite Foams for Electromagnetic Interference Shielding. *ACS Appl. Mater. Interfaces* **2013**, *5*, 2677−268.

(22) Shen, B.; Zhai, W. T.; Tao, M.; Ling, J.; Zheng, W. G. Lightweight, Multifunctional Polyetherimide/Graphene@Fe_3O_4 Composite Foams for Shielding of Electromagnetic Pollution. *ACS Appl. Mater. Interfaces* **2013**, *5*, 11383−11387.

(23) Ameli, A.; Jung, P. U.; Park, C. B. Electrical Properties and Electromagnetic Interference Shielding Effectiveness of Polypropylene/Carbon Fiber Composite Foams. *Carbon* **2013**, *60*, 379−391.

(24) Ameli, A.; Nofar, M.; Wang, S.; Park, C. B. Lightweight Polypropylene/Stainless-Steel Fiber Composite Foams with Low Percolation for Efficient Electromagnetic Interference Shielding. *ACS Appl. Mater. Interfaces* **2014**, *6*, 11091−11100.

(25) Bernal, M. M.; Mario-Gallego, M.; Molenberg, I.; Huynen, I.; Manchado, M. A. L.; Verdejo, R. Influence of Carbon Nanoparticles on the Polymerization and EMI Shielding Properties of PU Nanocomposite Foams. *RSC Adv.* **2014**, *4*, 7911−7918.

(26) Yang, W. R.; Qu, L. T.; Zheng, R. K.; Liu, Z. W.; Ratinac, K. R.; Shen, L. M.; Yu, D. S.; Yang, L.; Barrow, C. J.; Ringer, S. P.; Dai, L. M.; Braet, F. Self-Assembly of Gold Nanowires along Carbon Nanotubes for Ultrahigh-Aspect-Ratio Hybrids. *Chem. Mater.* **2011**, *23*, 2760−2765.

(27) Gelves, G. A.; Lin, B.; Sundararaj, U.; Haber, J. A. Low Electrical Percolation Threshold of Silver and Copper Nanowires in Polystyrene Composites. *Adv. Funct. Mater.* **2006**, *16*, 2423−2430.

(28) Gelves, G. A.; Al-Saleh, M. H.; Sundararaj, U. Highly Electrically Conductive and High Performance EMI Shielding Nanowire/Polymer Nanocomposites by Miscible Mixing and Precipitation. *J. Mater. Chem.* **2011**, *21*, 829−836.

(29) Zilberberg, K.; Gasse, F.; Pagui, R.; Polywka, A.; Behrendt, A.; Trost, S.; Heiderhoff, R.; Görrn, P.; Riedl, T. Highly Robust Indium-Free Transparent Conductive Electrodes Based on Composites of Silver Nanowires and Conductive Metal Oxides. *Adv. Funct. Mater.* **2014**, *24*, 1671−1678.

(30) Li, Y.; Cui, P.; Wang, L. Y.; Lee, H.; Lee, K.; Lee, H. Highly Bendable, Conductive, and Transparent Film by an Enhanced Adhesion of Silver Nanowires. *ACS Appl. Mater. Interfaces* **2013**, *5*, 9155−9160.

(31) Kim, T.; Canlier, A.; Kim, G. H.; Choi, J.; Park, M.; Han, S. M. Electrostatic Spray Deposition of Highly Transparent Silver Nanowire Electrode on Flexible Substrate. *ACS Appl. Mater. Interfaces* **2013**, *5*, 788−794.

(32) Hu, M. J.; Gao, J. F.; Dong, Y. C.; Li, K.; Shan, G. C.; Yang, S. L.; Li, R. K. Y. Flexible Transparent PES/Silver Nanowires/PET Sandwich-Structured Film for High-Efficiency Electromagnetic Interference Shielding. *Langmuir* **2012**, *28*, 7101−7106.

DOI: 10.1021/am5067095
ACS Appl. Mater. Interfaces 2015, 7, 563−576

(33) Yu, Y. H.; Ma, C. C. M.; Teng, C. C.; Huang, Y. L.; Lee, S. H.; Wang, I.; Wei, M. H. Electrical, Morphological, and Electromagnetic Interference Shielding Properties of Silver Nanowires and Nanoparticles Conductive Composites. *Mater. Chem. Phys.* **2012**, *136*, 334−340.
(34) Ma, J. J.; Zhan, M. S. Rapid Production of Silver Nanowires Based on High Concentration of $AgNO_3$ Precursor and Use of $FeCl_3$ as Reaction Promoter. *RSC adv.* **2014**, *4*, 21060−21071.
(35) Liu, X. Y.; Zhan, M. S.; Wang, K.; Li, Y.; Bai, Y. F. Preparation and Performance of a Novel Polyimide Foam. *Polym. Adv. Technol.* **2012**, *23*, 677−685.
(36) Liu, X. Y.; Zhan, M. S.; Wang, K. Preparation and Characterization of Electromagnetic Interference Shielding Polyimide Foam. *J. Appl. Polym. Sci.* **2013**, *127*, 4129−4137.
(37) Ma, J. J.; Zhan, M. S.; Wang, K. Facile Fabrication of Polyimide Foam Sheets with Millimeter Thickness: Processing, Morphology, and Properties. *J. Appl. Polym. Sci.* **2014**, *131*, 39881.
(38) Saeed, M. B.; Zhan, M. S. Adhesive Strength of Partially Imidized Thermoplastic Polyimide Films in Bonded Joints. *Int. J. Adhes. Adhes.* **2007**, *27*, 9−19.
(39) Joshi, A.; Bajaj, A.; Singh, R.; Alegaonkar, P. S.; Balasubramanian, K.; Datar, S. Graphene Nanoribbon-PVA Composite as EMI Shielding Material in the X band. *Nanotechnology* **2013**, *24*, 455705.
(40) Al-Saleh, M. H.; Sundararaj, U. X-band EMI Shielding Mechanisms and Shielding Effectiveness of High Structure Carbon Black/Polypropylene Composites. *J. Phys. D: Appl. Phys.* **2013**, *46*, 035304.
(41) Song, W. L.; Cao, M. S.; Hou, Z. L.; Lu, M. M.; Wang, C. Y.; Yuan, J.; Fan, L. Z. Beta-Manganese Dioxide Nanorods for Sufficient High-Temperature Electromagnetic Interference Shielding in X-band. *Appl. Phys. A: Mater. Sci. Process.* **2014**, *116*, 1779−1783.
(42) Cao, X.; James, L. L.; Widya, T.; Macosko, C. Polyurethane/Clay Nanocomposites Foams: Processing, Structure and Properties. *Polymer* **2005**, *46*, 775−783.
(43) Li, Y.; Ragauskas, A. J. Ethanol Organosolv Lignin-based Rigid Polyurethane Foam Reinforced with Cellulose Nanowhiskers. *RSC Adv.* **2012**, *2*, 3347−3351.
(44) Madaleno, L.; Pyrz, R.; Crosky, A.; Jensen, L. R.; Rauhe, J. C. M.; Dolomanova, V.; Timmons, A. M. V. B.; Pinto, J. J. C.; Norman, J. Processing and Characterization of Polyurethane Nanocomposite Foam Reinforced with Montmorillonite−Carbon Nanotube Hybrids. *Compos. Part A* **2013**, *44*, 1−7.
(45) Thomassin, J. M.; Pagnoulle, C.; Bednarz, L.; Huynen, I.; Jerome, R.; Detrembleur, C. Foams of Polycaprolactone/MWNT Nanocomposites for Efficient EMI Reduction. *J. Mater. Chem.* **2008**, *18*, 792−796.
(46) Li, C. Q.; Yang, G. H.; Deng, H.; Wang, K.; Zhang, Q.; Chen, F.; Fu, Q. The Preparation and Properties of Polystyrene/Functionalized Graphene Nanocomposite Foams Using Supercritical Carbon Dioxide. *Polym. Int.* **2013**, *62*, 1077−1084.
(47) Tran, M. P.; Detrembleur, C.; Alexandre, M.; Jerome, C.; Thomassin, J. M. The Influence of Foam Morphology of Multi-walled Carbon Nanotubes/Poly(methyl methacrylate) Nanocomposites on Electrical Conductivity. *Polymer* **2013**, *54*, 3261−3270.
(48) Pardo-Alonso, S.; Solórzano, E.; Estravís, S.; Rodríguez-Perez, M. A.; de Saja, J. A. In Situ Evidence of the Nanoparticle Nucleating Effect in Polyurethane−Nanoclay Foamed Systems. *Soft Matter* **2012**, *8*, 11262−11270.
(49) Bahrambeygi, H.; Rabbi, A.; Nasouri, K.; Shoushtari, A. M.; Babaei, M. R. Morphological and Structural Developments in Nanoparticles/Polyurethane Foam Nanocomposite's Synthesis and Their Effects on Mechanical Properties. *Adv. Polym. Tech* **2013**, *32*, 545−555.
(50) Bernala, M. M.; Pardo-Alonso, S.; Solórzano, E.; Lopez-Manchadoa, M. A.; Verdejo, R.; Rodríguez-Perez, M. A. Effect of Carbon Nanofillers on Flexible Polyurethane Foaming From a Chemical and Physical Perspective. *RSC Adv.* **2014**, *4*, 20761−20768.
(51) Harikrishnan, G.; Lindsay, C. I.; Arunagirinathan, M. A.; Macosko, C. W. Probing Nanodispersions of Clays for Reactive Foaming. *ACS Appl. Mater. Interfaces* **2009**, *1*, 1913−1918.
(52) Harikrishnan, G.; Patro, T. U.; Khakhar, D. V. Polyurethane Foam-Clay Nanocomposites: Nanoclays as Cell Openers. *Ind. Eng. Chem. Res.* **2006**, *45*, 7126−7134.
(53) Xu, Z. H.; Niu, Y. H.; Wang, Z. G.; Li, H.; Yang, L.; Qiu, J.; Wang, H. Enhanced Nucleation Rate of Polylactide in Composites Assisted by Surface Acid Oxidized Carbon Nanotubes of Different Aspect Ratios. *ACS Appl. Mater. Interfaces* **2011**, *3*, 3744−3753.
(54) Xu, D. H.; Wang, Z. G. Influence of Carbon Nanotube Aspect Ratio on Normal Stress Differences in Isotactic Polypropylene Nanocomposite Melts. *Macromolecules* **2008**, *41*, 815−825.
(55) Shirale, D. J.; Bangar, M. A.; Chen, W.; Myung, N. V.; Mulchandani, A. Effect of Aspect Ratio (Length:Diameter) on a Single Polypyrrole Nanowire FET Device. *J. Phys. Chem. C* **2010**, *114*, 13375−13380.
(56) Kim, H. R.; Kim, B. S.; Kim, I. S. Fabrication and EMI Shielding Effectiveness of Ag-decorated Highly Porous Poly(vinyl alcohol)/Fe_2O_3 Nanofibrous Composites. *Mater. Chem. Phys.* **2012**, *135*, 1024−1029.
(57) Kim, H. R.; Fujimori, K.; Kim, B. S.; Kim, I. S. Lightweight Nanofibrous EMI Shielding Nanowebs Prepared by Electrospinning and Metallization. *Compos. Sci. Technol.* **2012**, *72*, 1233−1239.
(58) Thomassin, J. M.; Jéróme, C.; Pardoen, T.; Bailly, C.; Huynen, I.; Detrembleur, C. Polymer/Carbon based Composites as Electromagnetic Interference (EMI) Shielding Materials. *Mater. Sci. Eng. R* **2013**, *74*, 211−232.
(59) Chen, Y.; Li, Y.; Yip, M.; Tai, N. Electromagnetic Interference Shielding Efficiency of Polyaniline Composites Filled with Graphene Decorated with Metallic Nanoparticles. *Compos. Sci. Technol.* **2013**, *80*, 80−86.
(60) Kwon, S.; Ma, R.; Kim, U.; Choi, H. R.; Baik, S. Flexible Electromagnetic Interference Shields Made of Silver Flakes, Carbon Nanotubes and Nitrile Butadiene Rubber. *Carbon* **2014**, *68*, 118−124.
(61) Zhang, C. S.; Ni, Q. Q.; Fu, S. Y.; Kurashiki, K. Electromagnetic Interference Shielding Effect of Nanocomposites with Carbon Nanotube and Shape Memory Polymer. *Compos. Sci. Technol.* **2007**, *67*, 2973−2980.
(62) Bergin, S. M.; Chen, Y. H.; Rathmell, A. R.; Charbonneau, P.; Li, Z. Y.; Wiley, B. J. The Effect of Nanowire Length and Diameter on the Properties of Transparent, Conducting Nanowire Films. *Nanoscale* **2012**, *4*, 1996−2004.
(63) Villacorta, B. S.; Ogale, A. A.; Hubing, T. H. Effect of Heat Treatment of Carbon Nanofibers on the Electromagnetic Shielding Effectiveness of Linear Low Density Polyethylene Nanocomposites. *Polym. Eng. Sci.* **2013**, *53*, 417−423.
(64) Yousefi, N.; Sun, X.; Lin, X.; Shen, X.; Jia, J.; Zhang, B.; Tang, B.; Chan, M.; Kim, J. K. Highly Aligned Graphene/Polymer Nanocomposites with Excellent Dielectric Properties for High Performance Electromagnetic Interference Shielding. *Adv. Mater.* **2014**, *26*, 5480−5487.
(65) Chen, Z. P.; Xu, C.; Ma, C. Q.; Ren, W. C.; Cheng, H. M. Light Weight and Flexible Graphene Foam Composites for High-Performance Electromagnetic Interference Shielding. *Adv. Mater.* **2013**, *25*, 1296−1300.

DOI: 10.1021/am5067095
ACS Appl. Mater. Interfaces 2015, 7, 563−576